Composites: Part A 190 (2025) 108542

Contents lists available at ScienceDirect

Composites Part A

journal homepage: www.elsevier.com/locate/compositesa

A simplified methodology for assessing the interface of CFRPs with fibre push-out testing

Dimitrios Gaitanelis [a,*], Craig J. Williams [b], Jack Donoghue [b], Clara Frias [a]

[a] Advanced Manufacturing Research Centre with Boeing, University of Sheffield, Catcliff, Rotherham S60 5TZ, UK
[b] The Henry Royce Institute, Department of Materials, University of Manchester, Manchester M13 9PL, UK

HIGHLIGHTS

- A simplified method is introduced for assessing the fibre/matrix interface of FRPs.
- Femtosecond laser processing is proposed for the specimen preparation.
- Nanoindentation fibre push-out testing is used for the mechanical assessment.
- The method captures the sizing agent effect on the interface of CFRPs.

GRAPHICAL ABSTRACT

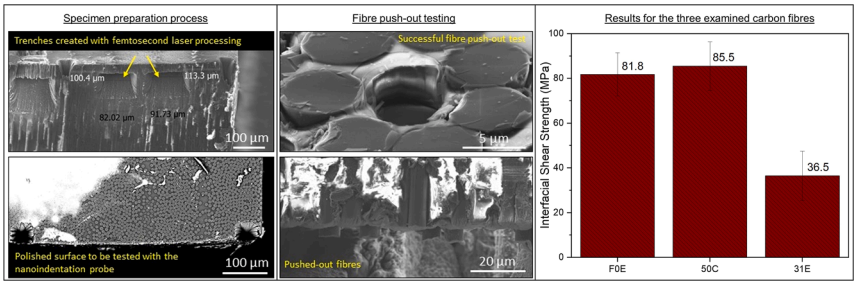

ARTICLE INFO

Keywords:
A. Polymer-matrix composites (PMCs)
A. Carbon fibres
B. Interface/interphase
B Fibre/matrix bond

ABSTRACT

This work proposes a simplified methodology for examining the interface of fibre reinforced composites with fibre push-out testing. Demonstrated in a carbon fibre (CF) reinforced polymer (CFRP) case study, it examines the interface of a commercial epoxy with the 31E, 50C, and F0E T700 CFs. Atomic force microscopy, attenuated total reflection – Fourier transform infrared spectroscopy, and scanning electron microscopy are used to characterise the fibres, and the CFRP samples are manufactured with wet winding. To create trenches of suitable thickness within the bulk composite, femtosecond-laser processing is proposed as a localised material subtractive method, facilitating the fibre push-out testing with the flat nanoindenter tip. The results highlight the influence of the CF sizing agent on the CFRP interface, and overall, a methodology is defined that simplifies the specimen preparation for assessing the interface of FRPs. This advancement holds promise for a broader adoption of such tests from both academia and industry.

1. Introduction

Fibre-reinforced polymer (FRP) composites offer not only high strength-to-weight ratio, but also exceptional properties such as high durability, stiffness, damping properties, flexural strength, resistance to corrosion, wear, and impact [1–3]. These diverse features have led these materials to find applications in construction, aerospace, automotive, biomedical, marine, and many other manufacturing industries [2]. Especially carbon fibre reinforced polymers (CFRPs) have advantageous mechanical, thermal, and chemical properties. Therefore, these materials are widely used in high-performance aerospace and automotive applications as substitutes for traditional metallic materials [4–7]. In a

* Corresponding author.
E-mail address: d.gaitanelis@sheffield.ac.uk (D. Gaitanelis).

https://doi.org/10.1016/j.compositesa.2024.108542
Received 20 June 2024; Received in revised form 14 October 2024; Accepted 20 October 2024
Available online 23 October 2024

CFRP material, the fibre provides the strength and the stiffness while the matrix is mainly responsible for transferring the stresses between the reinforcing fibres and safeguarding them from a mechanical and/or environmental damage.

Another attribute that significantly affects the mechanical performance of CFRPs is the fibre/matrix interface [8–12]. The interface plays a critical role in transferring the loads from the matrix to the fibres [13] and its resulting stress transfer efficiency determines the ultimate bulk material response [12]. Consequently, there is significant ongoing research focused on enhancing the interface of CFRPs [14,15]. Methods being explored include oxidation or plasma treatments of CFs [16–20], and the use of nanoparticles such as carbon nanotubes (CNTs) [21–25], graphitic carbon nitride (g-C3N4) [26] or graphene oxide (GO) [8,27] as coating layers. Additionally, modifications of the fibre's sizing agents are also being investigated [28–33].

To validate the benefits of these methodologies, it is important to employ reliable and robust experimental techniques. Nevertheless, to date a standard methodology for mechanically assessing the interface of FRPs has yet to be established [12,34]. For this reason, determining the interfacial shear strength (IFSS) of fibre-reinforced composites – the primarily studied parameter characterising the fibre/matrix interface – remains a challenge. Typically, single fibres are tested and the existing experimental methods can be divided into two main categories [13]. The first category involves tests where the external load is applied to the fibre such as single fibre pull-out tests (SFPTs) [32,35,36], microbond tests [37–42], fibre push-out tests [43–45], and fibre push-in tests [46]. The second category involves tests where the external load is applied to the matrix such as the Broutman test [47], and the single fibre fragmentation test (SFFT) [48,49]. Out of these tests, SFPTs, microbond tests, and fibre push-out tests are commonly used to examine the interface properties of FRPs [10–12,37,39,50–53].

Fibre push-out tests are lately increasingly employed from the research community to derive the IFSS of polymer matrix composites (PMCs) or ceramic matrix composites (CMCs) [34,51,53–57]. The main benefit of fibre push-out testing comparing to other methodologies is its ability to assess the IFSS in environments with increased fibre proximity. This approach can provide insights into the material response under conditions more representative of real-life manufacturing processes. Additionally, the testing process is relatively straightforward. Typically, it utilises a nanoindenter equipped with a flat punch indenter tip that applies the load to individual fibres until the interface failure initiates and the fibre push-out occurs [58].

The main barrier hindering a broader adoption of these tests in both industry and academia is the demanding specimen preparation process that is needed. In most cases, the thickness of the examined specimen should be less than 100 μm to ensure that debonding occurs along the fibre/matrix interface instead of fibre breakage [34,59,60]. To achieve that, the common practice is to hand grind and polish the samples. However, these manual methods are challenging, and usually result in premature sample breakage or uneven surfaces that hinder the effective contact between the fibre and the nanoindentation probe, therefore preventing the successful testing of the sample [60]. Hence, it is important to develop methodologies that simplify this process, facilitating the production of samples suitable for fibre push-out testing.

To address this gap, this study employs femtosecond (fs) laser processing to selectively ablate material beneath the sample's surface, thereby creating trenches within the bulk composite of suitable thickness for fibre push-out testing. This approach eliminates the requirement for extensive polishing and hand grinding, tackling the challenges associated with conventional specimen preparation methods. The applicability of the method is demonstrated by examining the interface bond of a thermosetting epoxy resin with three different commercial Toray T700 CFs. First, the CF surface is characterised using atomic force microscopy (AFM), attenuated total reflection – Fourier transform infrared spectroscopy (ATR-FTIR), and scanning electron microscopy (SEM). Subsequently, the interfaces of the three examined material systems are evaluated through fibre push-out testing. The results reveal the influence of the sizing agent on the IFSS, consistent with observations from the three fibre characterisation methods. In summary, this work presents and establishes a simplified methodology for examining the interface of fibre-reinforced composites with fibre push-out testing. Section 2 outlines the experimental process, section 3 discusses the results of the study, and section 4 gathers the main conclusions of this work.

2. Experimental

2.1. Materials

Three different types of commercial T700 CFs supplied by Toray Ltd., UK, are utilised in this work, namely, the T700SC-12 K-50C, the T700SC-12 K-F0E, and the T700GC-12 K-31E CFs with 1 %, 0.7 % and 0.5 % sizing agents (by weight), respectively [1,61]. The three examined fibres differ in sizing agents and sizing amounts, while the 50C and F0E CFs share the same fibre core (T700SC family). The 31E CF has a different fibre core (T700GS family) and according to the manufacturer it has also been surface treated [61] (Table 1). Regarding the resin, the material system used was the Araldite LY 556 epoxy resin combined with the XB 3473 formulated amine hardener provided by Mouldlife Ltd, UK.

2.2. Fibre characterization techniques

To characterise the surface of the CFs with the three different sizing agents, SEM, AFM, and ATR-FTIR are used. The SEM investigation focused on examining the effect of the sizing agent and of the sizing agent content on the surface morphology of the fibres using a JEOL 7900F scanning electron microscope available within the Henry Royce Institute, the University of Sheffield. Likewise, to examine the surface morphology at the nanoscale a Bruker Icon atomic force microscope available within the Henry Royce Institute, the University of Sheffield was used in the standard tapping mode in air. RTESPA-300 probes were utilised with an 8 nm tip radius, a 40 N/m spring constant, and 300 kHz resonant frequency. For each type of CF, several images were taken from different fibres with a scan rate of 0.498 Hz. The image size was set at 1 μm × 1 μm with a 512 × 512 pixels image resolution and the image processing took place using the NanoScope Analysis software. Height and phase images were captured for every fibre type and the average surface roughness (R_a) was measured using the "Roughness" function of the software. To minimise the influence of the fibre's curvature, the roughness measurements were performed in images that had undergone

Table 1
Examined carbon fibres.

Fibre type	Fibre core	Sizing type	Sizing amount, %	Surface treatment
T700SC-12 K-50C	T700SC	"5″	1	No
T700SC-12 K-F0E	T700SC	"F"	0.7	No
T700GC-12 K-31E	T700GC	"3″	0.5	Yes

flattening. To examine the functional groups on the surface of the three different fibres, an ATR-FTIR analysis took place in the Advanced Manufacturing Research Centre (AMRC), Sheffield, UK using a Perkin Elmer Spectrum 2 diamond ATR-FTIR. Five measurements took place for each fibre with a resolution of 2 cm^{-1} and a total of 20 scans and the spectra were collected from 4000 to 600 cm^{-1}. To analyse the results and identify the main functional groups of each fibre, the spectra were smoothed and baseline corrected.

2.3. Wet winding and oven curing

To manufacture the epoxy CFRP laminates with the three different CFs, wet winding was employed utilising the AMRC's 6-axis robotic filament winding system. The system includes a KUKA KR150 robot arm, a spring-loaded creel tensioning system and a carriage which mounts the chucks that hold and rotate the tooling (Fig. 1a, Fig. 1b). The laminates were wound onto a flat laminate tool, and to facilitate the removal and improve the surface finish a 350 mm × 350 mm aluminium caul plate was also mounted onto the tool (Fig. 1c). Following the manufacturer's recommendations, the mix ratio used was 100 parts per weight for the Araldite LY 556 epoxy resin and 23 parts per weight for the XB 3473 hardener and the winding took place with 10 % of the nominal winding speed and a doctor blade gap of 0.5 mm.

The wound laminates with the three different CFs underwent curing in a Caltherm oven according to the following program: a ramp at 2 °C/min to 120 °C, followed by a 2-hour dwell at 120 °C, then a ramp at 1 °C/min to 180 °C with a 4-hour dwell at 180 °C, and finally a ramp at 3 °C/min to 40 °C. Upon completion, the cured CFRP laminates of Fig. 1d were removed from the tool and were then used for preparing the specimens suitable for fibre push-out testing.

2.4. Specimen preparation: Initial polishing and fs-laser milling

To prepare the samples for fibre push-out testing, specimens were cut with a diamond saw at an approximate size of 20 mm × 20 mm. The cut samples were then cold mounted and the surface vertical to the fibres was mechanically ground and polished using the Struers LaboPol-30/LaboForce-50. The applied polishing procedure involved a 1200 grinding paper, followed by grinding disks with diamond suspension of 9 μm and 3 μm respectively, and finally a 1 μm polishing cloth with a 0.04 μm colloidal silica suspension. Upon completion, each sample was removed from the mounted resin and was then sectioned into two 10 mm × 20 mm samples. To achieve a flat and uniform surface for the fs-laser milling, the cut edge with the unidirectionally aligned fibres underwent manual polishing using an 800 grit paper followed by a 2400 grit paper and finished with the 1 μm polishing cloth with a 0.04 μm colloidal silica suspension. To ensure that the samples' surface was appropriate for push-out testing the samples were assessed with optical microscopy and were then sputter coated and mounted on cylindrical pins.

The fs-laser subtractive process took place with a Thermo Scientific Laser PFIB located within the Henry Royce Institute, The University of Manchester. The system has been more fully described in [62] and consists of a femtosecond laser mounted so that the laser ablation point, electron imaging, and focused ion beam are all coincident within the SEM chamber. Overall, the ultra-short pulses utilised during fs-laser milling primarily ablate the material minimising the thermal conduction, thereby resulting in a nominal heat-affected zone (HAZ) [34,63]. In this work, the laser milling took place with a laser wavelength of 515 nm, a pulse duration of ~ 300 fs and an energy of 10 μJ. The pulse was fired with a frequency of 60 kHz, and to mill the trench the beam was rastered over an area of 100 μm by 50 μm with a pitch in x and y of 1 μm (95 % overlap for the measured ablated spot diameter of 20 μm). The

Fig. 1. Panels manufacturing schematic: a) 6-axis robotic filament winding system, b) wet winding bath set up c) flat laminate tool with a 350 mm × 350 mm caul plate, and d) cured laminates with the three different fibres.

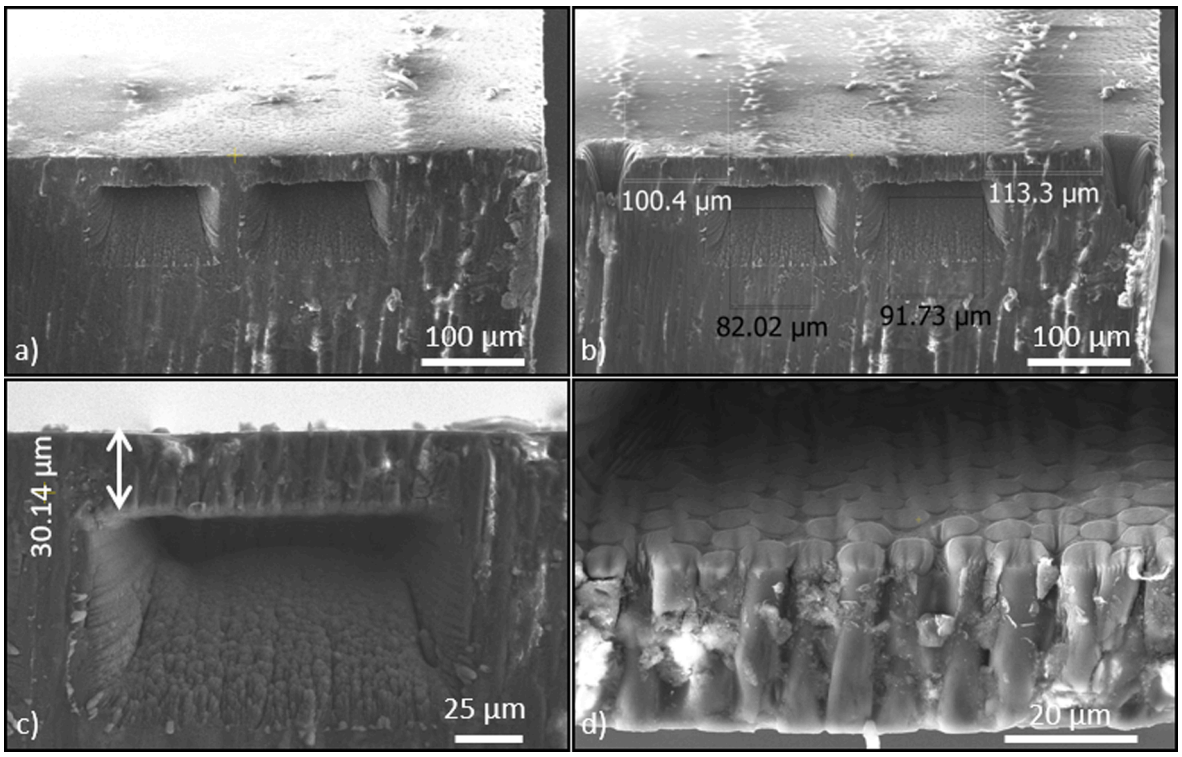

Fig. 2. Created trenches within the bulk composite using fs-laser processing: a) trenches, b) material marks indicating the testing region, c) thickness measurement, and d) surface quality within the created trench (upside down figure).

pulse was allowed to fire 20 times in each location before moving on to the next step of the raster for a total time laser processing of 10 s per trench.

Fig. 2 shows the resultant trenches with their openings measuring ~ 120 µm by 70 µm and their depth estimated around 80 µm. The target thickness of the resulting testing region varied from 30 µm to 45 µm (Fig. 2). Thicker regions could lead to fibre fracture or matrix damage, and regions < 30 µm could induce bending stresses on the material, while the target thickness used resulted in successful fibre push-outs. To ensure a consistent thickness for the tested region, the laser ablation was carried out at 12° incidence to account for the inherent taper of the laser milling process. Additionally, to successfully test the milled region with the nanoindenter the bulk material proximal to the trenches was marked on the top surface (Fig. 2b). Finally, as expected, no apparent thermal damage was observed in the vicinity of the trenches.

2.5. Single fibre push-out tests

After creating the trenches, the fibre/matrix interface of the examined samples was assessed with fibre push-out tests. The tests were performed in the Nanocharacterisation Laboratory, part of the Royce Institute based at The University of Manchester. A Bruker Hysitron Ti980 (Bruker Hysitron, Minneapolis, MN, USA) nanoindenter was used equipped with a flat punch indenter tip of a 4 µm diameter and a 60° conical angle. The fibres were tested at a displacement rate of 24 nm/s and an indentation depth of 5.5 µm. The test's main output is the value of the apparent IFSS, which is calculated by

$$Apparent\ IFSS = \frac{F_{max}}{\pi D_f L_e} \quad (1)$$

where F_{max} is the maximum load that occurs in debonding. L_e is the embedded fibre length which equals the thickness of the material left above the trench (Fig. 2c), while D_f stands for the fibre diameter that is measured with SEM after the performed tests. It should be noted that this method evaluates the apparent IFSS rather than the true local IFSS. The apparent IFSS includes an unknown frictional contribution, as the calculation is based solely on the maximum applied force at the moment of debonding, without accounting for the non-uniform interfacial shear that occurs along the embedded fibre length.

3. Results and discussion

3.1. Fibre characterisation: SEM, AFM, and ATR-FTIR

3.1.1. SEM

Fig. 3 shows the surface morphology of representative CFs of each examined fibre type as captured with SEM. The results show that the different sizing agent/sizing agent content alters the CF surface morphology. First, bumps are noticed in the 50C CF where a 1 % sizing agent is used (Fig. 3a), which are attributed to the aggregated polymeric sizing [2]. On the other hand, linear marks are evident on the surface of the F0E CF with a 0.7 % sizing content (Fig. 3b). These marks result from the manufacturing method that is used for the F0E CFs [2]. Finally, the 31E CF shows the most uniform surface due to the smaller amount of sizing agent that it has – equal to 0.5 % (Fig. 3c).

3.1.2. AFM

To provide a greater detail on the SEM observations, an AFM investigation takes place where the surface morphology of the examined fibres is assessed in the nanoscale and their surface roughness is also quantified. Fig. 4 shows representative AFM height and phase images of the three different fibre types. The height images indicate that the surface of the 50C fibres – the fibres with the highest amount of sizing agent – is dominated by the polymeric agglomerates of the sizing agent (Fig. 4a). Likewise, but to a lesser extent, the F0E CFs also have numerous agglomerates on their surface (Fig. 4b), while the 31E CFs with the lowest amount of sizing agent display a more uniform surface in their height images (Fig. 4c).

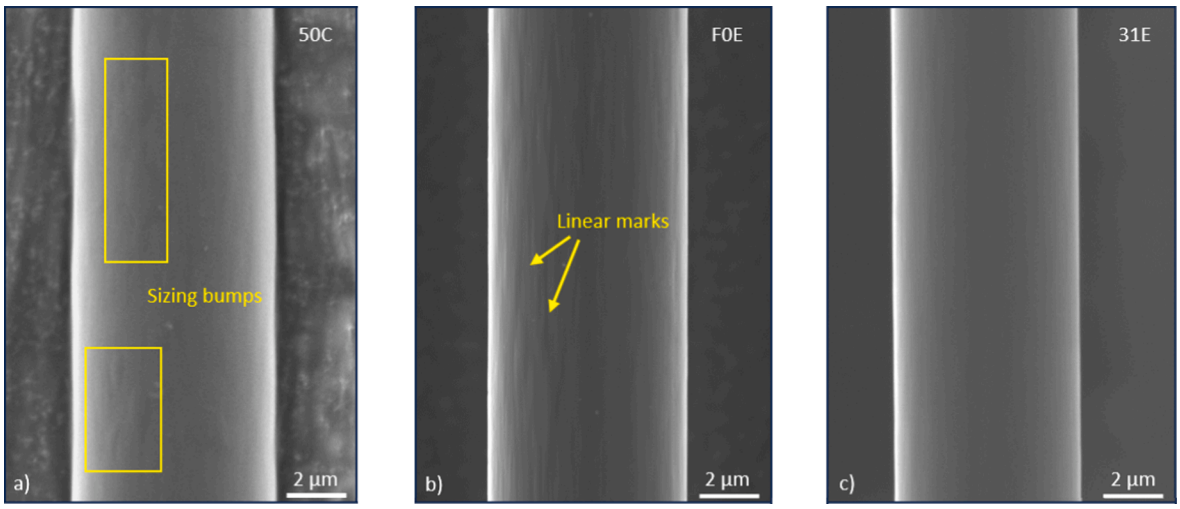

Fig. 3. Representative SEM imaging of the three examined carbon fibre types: a) 50C, b) F0E, and c) 31E.

These results are corroborated by surface roughness measurements, which revealed an average surface roughness of 2.82 nm for the 50C CFs, 2.65 nm for the F0E CFs, and 0.98 nm for the 31E CFs. To obtain these values, up to three different regions were examined for each fibre type. As discussed in section 2.2, the analysis was conducted on images that had undergone flattening to minimise the influence of the fibre's curvature and accurately measure the roughness due to the nano-structures along the fibre surface. Overall, the results highlight significant differences in the surface morphology and roughness of the examined fibres. Interestingly, as shown by the fibre push-out tests, these variations have a substantial impact on the mechanical and chemical interlocking of the fibres with the examined epoxy resin. Specifically, a stronger interface bond was formed with the 50C and F0E CFs compared to the 31E CFs (Fig. 11).

Finally, the AFM phase images also indicate the disparities in the surface morphology. Utilising color contrast, these images depict variations in phase angle across each sample's surface. These phase angle discrepancies are indicative of the sample's viscoelastic properties, highlighting the differences that exist within the material composition [1]. However, it's worth noting that these variations are also influenced by the sample's surface morphology. Indeed, differences in phase images among the three fibre types are noticed in regions where the surface morphology is altered in this work (Fig. 4). Therefore, the analysis suggests uniform viscoelastic properties across the surface of the examined fibres, given the minimal contrast elsewhere in the images [1].

3.1.3. ATR-FTIR

To detect the functional groups on the surface of the examined fibres, ATR-FTIR is used, and the accumulated transmittance spectra are presented in Fig. 5. A consistent finding across the three examined fibre types are the peaks at 2166 cm^{-1} and 2114 cm^{-1}. These peaks are attributed to the existence of azides (R-N_3) and alkyne (RC≡CR′) functional groups respectively [2]. Azides are particularly important as curing agents for epoxy resin systems, as they can undergo conversion into primary amines (RNH2) [2]. The latter are widely recognized as effective hardeners. For instance, as discussed in section 2.1, the XB 3473 hardener utilised in this study is also a formulated amine hardener.

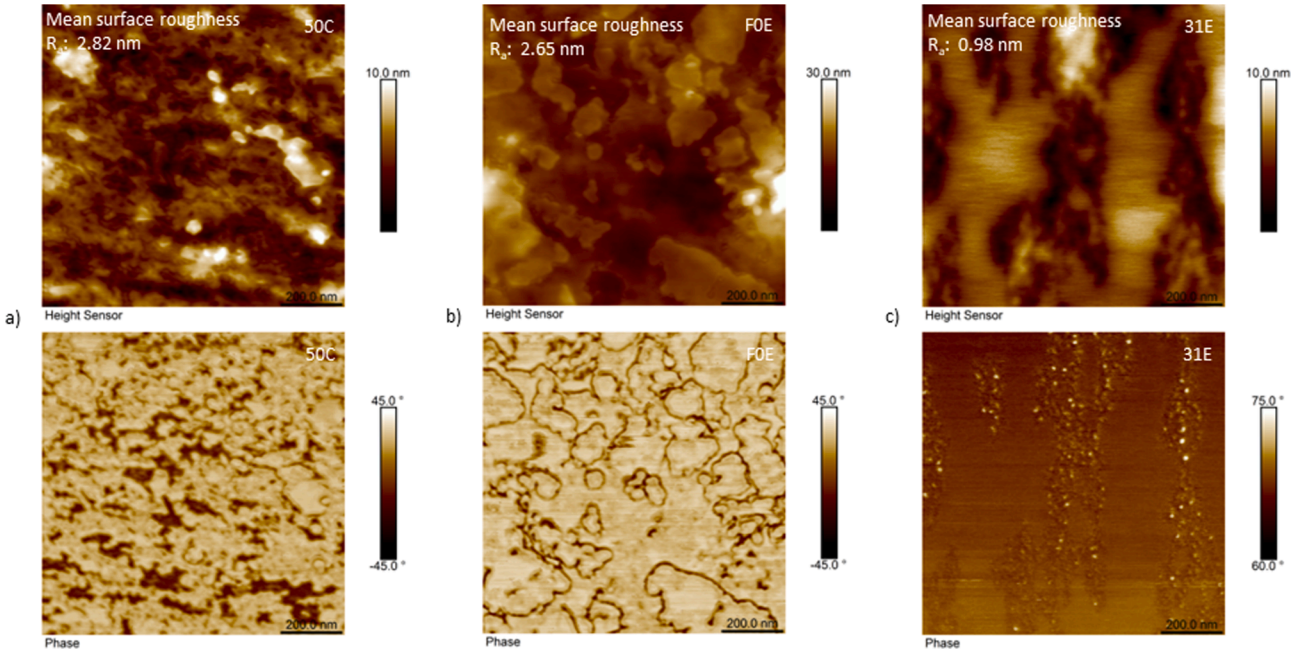

Fig. 4. Representative AFM height (top) and phase (bottom) images for the three examined fibre types: a) 50C, b) F0E, c) 31E.

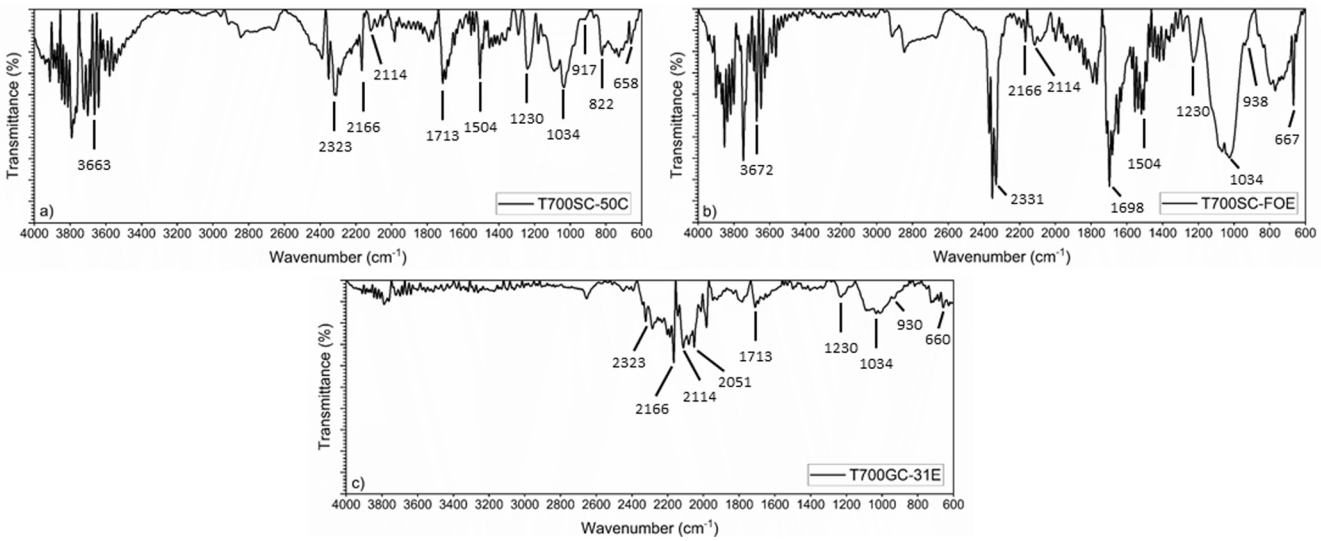

Fig. 5. FTIR spectra of the examined carbon fibres: a) 50C, b) F0E, c) 31E.

Additionally, the peaks found at 1713 cm^{-1} (50C & 31E) and 1698 cm^{-1} (F0E) reveal the presence of carboxylic acid (RCOOH) and of ketone groups in the three examined fibres, while the 1230 cm^{-1} peak together with the bands at 917 cm^{-1} (50C), 938 cm^{-1} (F0E), and 930 cm^{-1} (31E) are indicative of stretching vibrations in epoxy compounds (RCOOR') [2].

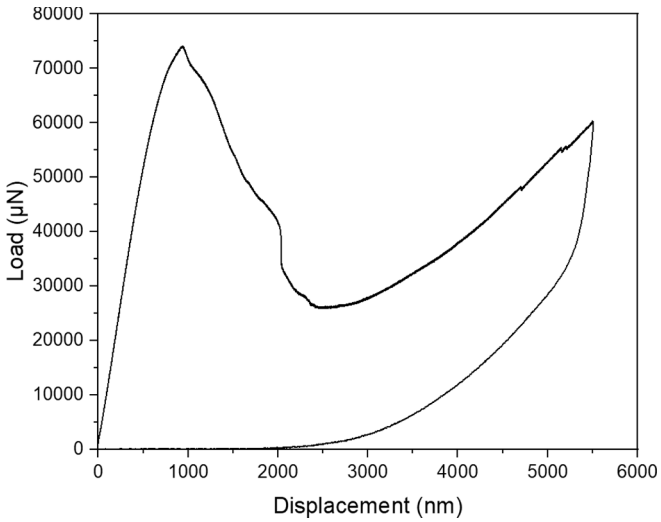

Fig. 6. Typical load–displacement curve of a successful fibre push-out test.

Contrary to these consistent findings, bands in the 3700–3200 cm^{-1} spectral region are noticed in the 50C and F0E fibres with strong peaks at around 3660 cm^{-1}. These bands correspond to the stretching of the hydroxyl groups (ROH) [2], and are not present in the 31E fibre (Fig. 5c). Additionally, N—H vibrations are identified at 3500–2300 cm^{-1} with stronger adsorption in the 50C and F0E fibres than in the 31E fibre. Interestingly, previous studies have found that a higher presence of N groups can enhance the crosslinking density in epoxy resin systems due to their significant functionality [2,64]. Likewise, the 1504 cm^{-1} peak, noted only in the 50C and F0E fibres, indicates the presence of aromatic nitro compounds (RNO_2). The active hydrogen that is present in these compounds can also enhance the crosslinking that occurs in these fibres.

Altogether, similarly to previous studies [2,65–67], the FTIR analysis of this work highlights the slight differences in the functional groups of the examined fibre types. These variations could impact the bonding with the tested resin. Finally, when these findings are considered alongside the SEM and AFM observations, they could explain the enhanced adhesion of the resin with the 50C and F0E carbon fibres compared to the 31E fibre (Fig. 11).

3.2. *Single fibre push-out tests*

Fig. 6 shows a typical load displacement curve of the performed fibre push-out tests. The maximum load, Fmax, is where the push-out takes place. After the push-out, with a further increase of the indentation depth the load decreases until reaching a point where the conical tip contacts the surrounding matrix, resulting in the subsequent load

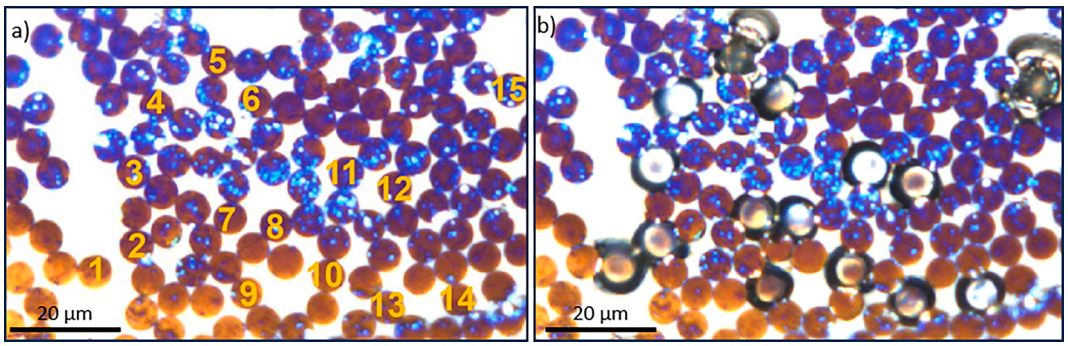

Fig. 7. Tested fibres before and after the performed fibre push-out tests, as captured by the optical microscope of the nanoindenter.

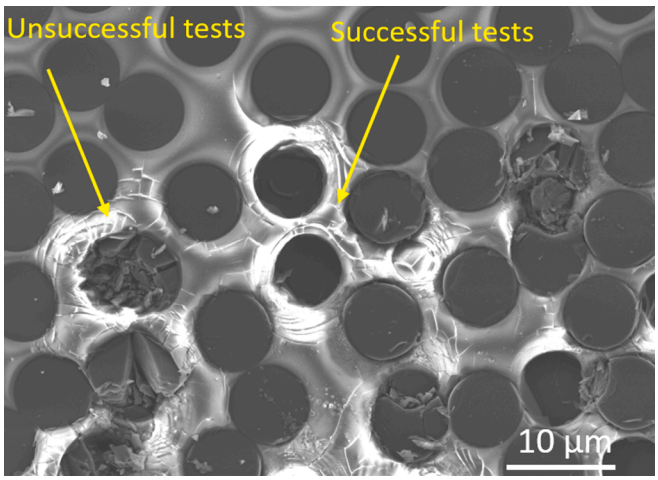

Fig. 8. Examples of successful and unsuccessful push-out tests in the examined samples.

increase observed in the graph. Altogether, 9–20 fibres were tested in each sample and a visual representation of the fibres before and after testing – as captured by the optical microscope of the nanoindenter – is first shown in Fig. 7.

To verify the success of each test, the tested samples are further investigated with SEM and examples of successful and unsuccessful tests are presented in Fig. 8. The main reason behind the unsuccessful tests of Fig. 8 is the misalignment between the testing probe and the fibres. On the other hand, a properly centered tip results in successful fibre push-out and a more detailed observation of the resulting failure modes is shown in Fig. 9. Fig. 9a and Fig. 9b clearly illustrate the event of fibre/matrix debonding that takes place on these tests. Opposite to that, fibre damage is evident in Fig. 9c, attributed to the misalignment of the testing probe with the examined fibres. To further demonstrate the event of fibre push-out in the examined samples, Fig. 9d and Fig. 9e present typical SEM images of pushed-out fibres within the examined trench.

Taken together, the analysis shows that the specimen preparation process followed in this work consists of an efficient method for preparing samples suitable for fibre push-out testing. As discussed, the main outcome of these tests is the value of the apparent IFSS which is the predominately examined property for characterising the fibre/matrix interface in composites [12]. To calculate this value for each tested fibre, the maximum load F_{max} is derived from the load displacement curve and the fibre diameter D_f is measured with SEM. Examples of this process are shown in Fig. 10, and after applying the values of each tested fibre in Eq. (1), the average IFSS is calculated for the three reinforced samples with the different CFs.

Fig. 11 shows that the strongest interface bond is observed in the 50C sample, achieving an apparent IFSS of 85.5 ± 10.8 MPa. A 4.35 % decrease is noticed at the F0E sample, resulting in an apparent IFSS of

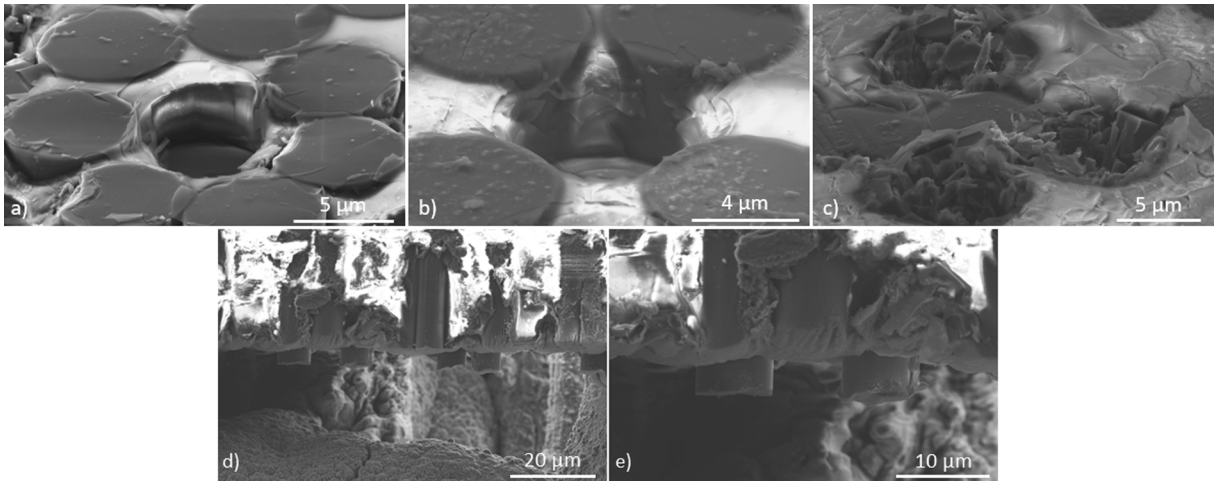

Fig. 9. a, b) successful fibre push-out tests showcasing the resulting fibre/matrix debonding, c) unsuccessful tests resulting in fibre damage due to the misalignment of the indenter tip & d, e) pushed-out fibres within the examined trench as captured with SEM.

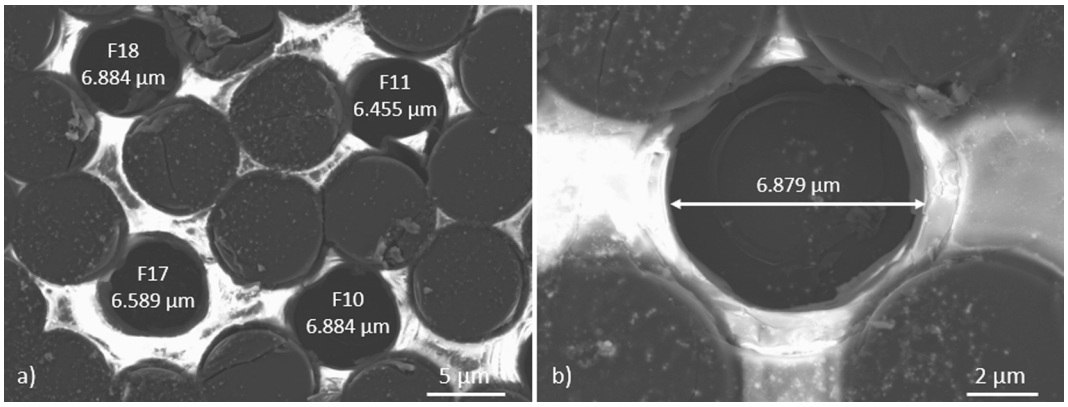

Fig. 10. Measuring the fibre diameter of the pushed-out fibres: a) meso level, b) detail.

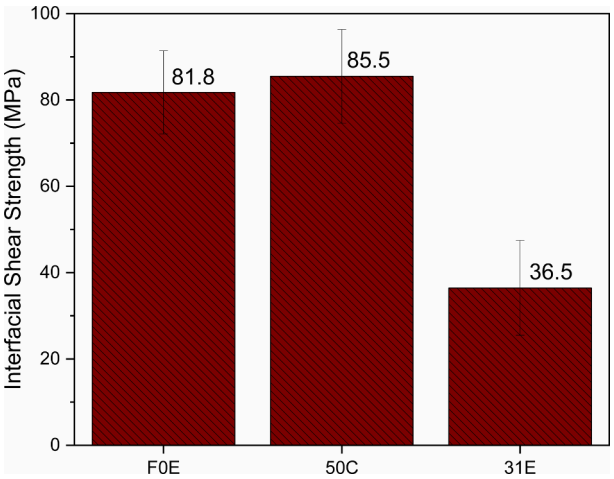

Fig. 11. Apparent IFSS of the LY 556 epoxy resin when reinforced with the three examined CFs.

81.8 ± 9.6 MPa, while the weakest bond is found when the resin is reinforced with the T700GS – 31E CF reaching an apparent IFSS of 36.5 ± 11 MPa (Table 2). Although the number of fibres tested varies across the groups (Table 2), previous studies have demonstrated that as few as 5 successful tests can produce reliable IFSS results [12]. Consequently, the number of successful push-out tests in each group provides a statistically sound basis for confidence in the obtained values. Moreover, the similar standard deviations across the three groups suggest consistent data dispersion. Finally, to validate the statistical significance of the observed IFSS change, an analysis of variance (ANOVA) is conducted at a 99 % confidence level (p-value < 0.01). Indeed, for the three examined groups of fibres, the null hypothesis is rejected (p-value < 0.00001), indicating a 99 % confidence that the observed IFSS change accurately represents a genuine alteration in the interface properties of the examined resin when reinforced with the three different CFs (Table 2).

It should be noted that the IFSS results of Fig. 11 are consistent with the SEM, AFM, and ATR-FTIR findings of this work. SEM and AFM revealed a less uniform surface on the 50C and F0E fibres. This was attributed to the higher sizing agent content that these fibres have compared to the 31E fibres. As previously highlighted, this less uniform surface favors their bonding with the examined resin material system. Likewise, ATR-FTIR captured slight differences in the chemical distribution of the functional groups on the surface of the three fibre types. As discussed in section 3.1.1, these variations also suggest a stronger bonding affinity of the 50C and F0E fibres compared to the 31E fibres. These observations are directly reflected in the IFSS values, which show that the higher sizing content of the 50C and F0E fibres enhances their interfacial adhesion with the examined resin (Fig. 11). Finally, the lower IFSS values for the 31E fibres may also be influenced by their distinct surface treatment and core material, likely contributing to an overall weaker interface bond.

4. Conclusions

The fibre/matrix interface significantly influences the mechanical performance of fibre-reinforced composites, prompting ongoing research on interface enhancement methods. Nevertheless, to date, a standardised approach for mechanically evaluating the interface of FRPs has not been established, making the determination of interfacial shear strength challenging. This work addresses this gap by proposing a simplified approach that employs femtosecond laser processing for specimen preparation and nanoindentation fibre push-out testing for mechanical assessment. The novelty of this study lies in the use of femtosecond laser processing to create trenches suitable for fibre push-out testing (<50 μm thick), eliminating the need for extensive polishing and significantly streamlining the testing process. The method's applicability was demonstrated by examining the interface bond of an epoxy resin system with three different commercially available carbon fibres.

The results indicate that the method effectively captures the influence of the sizing agent on the fibre/matrix interface bond. While we acknowledge that the method requires specific instrumentation, it significantly reduces preparation time compared to conventional specimen preparation methods, offering a more efficient approach for fibre push-out testing. Moreover, with the growing availability of stand-alone femtosecond laser milling tools and the increasing use of integrated SEM/nanoindentation systems for such tests, the applicability of the proposed method is expected to expand further. Consequently, by simplifying the specimen preparation and testing process, this advancement can serve as a major incentive for the research community. It could enable a more widespread adoption of fibre push-out tests within both academia and industry, thereby augmenting the volume of research conducted in the field of composites interface.

CRediT authorship contribution statement

Dimitrios Gaitanelis: Writing – original draft, Visualization, Validation, Resources, Project administration, Methodology, Investigation, Funding acquisition, Formal analysis, Data curation, Conceptualization. **Craig J. Williams:** Writing – review & editing, Methodology, Investigation. **Jack Donoghue:** Writing – review & editing, Methodology, Investigation. **Clara Frias:** Writing – review & editing, Resources, Project administration, Funding acquisition.

Declaration of competing interest

The authors declare that they have no known competing financial interests or personal relationships that could have appeared to influence the work reported in this paper.

Table 2
Average IFSS, standard deviation, and number of tested fibres per group and summary of the ANOVA analysis for the three examined fibre types.

Fibre type	Apparent IFSS (MPa)	Successfully tested fibres / total number of tests
T700SC-12 K-50C	85.5 ± 10.8	19/20
T700SC-12 K-F0E	81.8 ± 9.6	11/15
T700GC-12 K-31E	36.5 ± 11	9/9

Analysis of Variance (ANOVA) summary

Source	Degrees of freedom (DF)	Sum of squares (SS)	Mean Square (MS)	F-stat	P-value
Between groups	2	15828.5109	7914.2555		
Within groups	36	4000.6241	111.1284	71.21719	< 0.00001
Total	38	19829.135			

Acknowledgements

We wish to acknowledge the support of the Henry Royce Institute for advanced materials established through EPSRC Grants EP/R00661X/1, EP/P025498/1 and EP/P025021/1 and specifically through the Industrial Collaboration Programme, funded from a grant provided by the Engineering and Physical Sciences Research Council (EP/X527257/1).

We also wish to acknowledge Nexam Chemical St Andrews Ltd and particularly Boyd Cushing, Business Development Lead for the UK & Ireland, for their assistance and collaboration throughout the project.

We would also like to thank Dr Xinyue Chen from the Henry Royce Nanocharacterisation Laboratory at the University of Sheffield for the AFM work, Dr Le Ma from the Sorby Centre for Electron Microscopy at the University of Sheffield for the SEM work, and Andrew Forrest from the Henry Royce Nanomechanical Testing Laboratory at the University of Manchester for his support on the nanoindentation work.

Finally, the authors would like to acknowledge the contribution of the AMRC project team that worked on this project. In alphabetical order, special thanks go to Lewis Bower, Oleksii Brahinets, Robyn Elliott, Matthew J. Firth, Dr Gary M. Foster, Dr Andrew Patterson, Dr Matthew I. Smith, and Dr Anthony Stevenson.

Data availability

Data will be made available on request.

References

[1] Mamalis D, Murray JJ, McClements J, Tsikritsis D, Koutsos V, McCarthy ED, et al. Novel carbon-fibre powder-epoxy composites: interface phenomena and interlaminar fracture behaviour. Compos B Eng 2019;174:107012. https://doi.org/10.1016/j.compositesb.2019.107012.

[2] Mamalis D, Flanagan T, Brádaigh CMÓ. Effect of fibre straightness and sizing in carbon fibre reinforced powder epoxy composites. Compos Part A Appl Sci Manuf 2018;110:93–105. https://doi.org/10.1016/j.compositesa.2018.04.013.

[3] Gaitanelis DG, Giannopoulos IK, Theotokoglou EE. Numerical FEA parametric analysis of CAI behaviour of CFRP stiffened panels. Thin-Walled Struct 2019;143. https://doi.org/10.1016/j.tws.2019.106231.

[4] Pramanik A, Basak AK, Dong Y, Sarker PK, Uddin MS, Littlefair G, et al. Joining of carbon fibre reinforced polymer (CFRP) composites and aluminium alloys – a review. Compos Part A Appl Sci Manuf 2017;101:1–29. https://doi.org/10.1016/j.compositesa.2017.06.007.

[5] Gaitanelis D, Worrall C, Kazilas M. Detecting, characterising and assessing PEEK's and CF-PEEK's thermal degradation in rapid high-temperature processing. Polym Degrad Stab 2022;204:110096. https://doi.org/10.1016/j.polymdegradstab.2022.110096.

[6] Gaitanelis D, Worrall C, Kazilas M. A numerical model to prevent the thermal degradation of CFRPs at extreme heating rates – the laser processing of CF/PEEK. Compos Part A Appl Sci Manuf 2024;177:107938. https://doi.org/10.1016/j.compositesa.2023.107938.

[7] Courvoisier E, Bicaba Y, Colin X. Multi-scale and multi-technique analysis of the thermal degradation of poly(ether ether ketone). Polym Degrad Stab 2018;151:65–79. https://doi.org/10.1016/j.polymdegradstab.2018.03.001.

[8] Chen J, Wang K, Zhao Y. Enhanced interfacial interactions of carbon fiber reinforced PEEK composites by regulating PEI and graphene oxide complex sizing at the interface. Compos Sci Technol 2018;154:175–86. https://doi.org/10.1016/j.compscitech.2017.11.005.

[9] Li N, Chen J, Liu H, Dong A, Wang K, Zhao Y. Effect of preheat treatment on carbon fiber surface properties and fiber/PEEK interfacial behavior. Polym Compos 2019;40:E1407–15. https://doi.org/10.1002/pc.25020.

[10] Yang L, Thomason JL. Interface strength in glass fibre–polypropylene measured using the fibre pull-out and microbond methods. Compos Part A Appl Sci Manuf 2010;41:1077–83. https://doi.org/10.1016/j.compositesa.2009.10.005.

[11] Thomason JL. The interface region in glass fibre-reinforced epoxy resin composites: 2. Water absorption, voids and the interface. Composites 1995;26:477–85. https://doi.org/10.1016/0010-4361(95)96805-G.

[12] Gaitanelis D, Worrall C, Kazilas M. Influence of rapid high-temperature processing on the interface of CF/PEEK: a quick and effective method for enhancing the IFSS. Compos Sci Technol 2024:110564. https://doi.org/10.1016/j.compscitech.2024.110564.

[13] Zhandarov S, Mäder E. Characterization of fiber matrix interface strength applicability of different tests, approaches and parameters. Compos Sci Technol 2005;65:149–60. https://doi.org/10.1016/j.compscitech.2004.07.003.

[14] Zheng H, Zhang W, Li B, Zhu J, Wang C, Song G, et al. Recent advances of interphases in carbon fiber-reinforced polymer composites: a review. Compos B Eng 2022;233:109639. https://doi.org/10.1016/j.compositesb.2022.109639.

[15] Rohini R, Katti P, Bose S. Tailoring the interface in graphene/thermoset polymer composites: a critical review. Polymer (Guildf) 2015;70:A17–34. https://doi.org/10.1016/j.polymer.2015.06.016.

[16] Yu J, Meng L, Fan D, Zhang C, Yu F, Huang Y. The oxidation of carbon fibers through $K_2S_2O_8/AgNO_3$ system that preserves fiber tensile strength. Compos B Eng 2014;60:261–7. https://doi.org/10.1016/j.compositesb.2013.12.037.

[17] Chen Q, Peng Q, Zhao X, Sun H, Wang S, Zhu Y, et al. Grafting carbon nanotubes densely on carbon fibers by poly(propylene imine) for interfacial enhancement of carbon fiber composites. Carbon N Y 2020;158:704–10. https://doi.org/10.1016/j.carbon.2019.11.043.

[18] Finegan IC, Tibbetts GG, Glasgow DG, Ting J-M, Lake ML. Surface treatments for improving the mechanical properties of carbon nanofiber/thermoplastic composites. J Mater Sci 2003;38:3485–90. https://doi.org/10.1023/A:1025109103511.

[19] Pitto M, Fiedler H, Kim NK, Verbeek CJR, Allen TD, Bickerton S. Carbon fibre surface modification by plasma for enhanced polymeric composite performance: a review. Compos Part A Appl Sci Manuf 2024;180:108087. https://doi.org/10.1016/j.compositesa.2024.108087.

[20] Zhang H, Li W. Plasma-grafting polymerization on carbon fibers and its effect on their composite properties. Appl Surf Sci 2015;356:492–8. https://doi.org/10.1016/j.apsusc.2015.08.016.

[21] Xiao C, Tan Y, Wang X, Gao L, Wang L, Qi Z. Study on interfacial and mechanical improvement of carbon fiber/epoxy composites by depositing multi-walled carbon nanotubes on fibers. Chem Phys Lett 2018;703:8–16. https://doi.org/10.1016/j.cplett.2018.05.012.

[22] Lamorinière S, Jones MP, Ho K, Kalinka G, Shaffer MSP, Bismarck A. Carbon nanotube enhanced carbon Fibre-Poly(ether ether ketone) interfaces in model hierarchical composites. Compos Sci Technol 2022;221:109327. https://doi.org/10.1016/j.compscitech.2022.109327.

[23] Lyu H, Jiang N, Li Y, Lee H, Zhang D. Enhanced interfacial and mechanical properties of carbon fiber/PEEK composites by hydroxylated PEEK and carbon nanotubes. Compos Part A Appl Sci Manuf 2021;145:106364. https://doi.org/10.1016/j.compositesa.2021.106364.

[24] Lai M, Jiang L, Wang X, Zhou H, Huang Z, Zhou H. Effects of multi-walled carbon nanotube/graphene oxide-based sizing on interfacial and tribological properties of continuous carbon fiber/poly(ether ether ketone) composites. Mater Chem Phys 2022;276:125344. https://doi.org/10.1016/j.matchemphys.2021.125344.

[25] Li H, Peng Y, Li Z, Jiang Z, Zhang Q, Wu L. Plasma actuating modified multiwalled carbon nanotubes (MWCNTs) to strengthen interface of MWCNTs/Polylactic acid composites by constructing interlaminar stress-transfer bridge. Polym Test 2023;129:108261. https://doi.org/10.1016/j.polymertesting.2023.108261.

[26] Song B, Wang T, Sun H, Liu H, Mai X, Wang X, et al. Graphitic carbon nitride (g-C_3N_4) interfacially strengthened carbon fiber epoxy composites. Compos Sci Technol 2018;167:515–21. https://doi.org/10.1016/j.compscitech.2018.08.031.

[27] Azimpour-Shishevan F, Akbulut H, Mohtadi-Bonab MA. Synergetic effects of carbon nanotube and graphene addition on thermo-mechanical properties and vibrational behavior of twill carbon fiber reinforced polymer composites. Polym Test 2020;90:106745. https://doi.org/10.1016/j.polymertesting.2020.106745.

[28] Yan T, Yan F, Li S, Li M, Liu Y, Zhang M, et al. Interfacial enhancement of CF/PEEK composites by modifying water-based PEEK-NH2 sizing agent. Compos B Eng 2020;199:108258. https://doi.org/10.1016/j.compositesb.2020.108258.

[29] Ma Y, Yokozeki T, Ueda M, Sugahara T, Yang Y, Hamada H. Effect of polyurethane dispersion as surface treatment for carbon fabrics on mechanical properties of carbon/Nylon composites. Compos Sci Technol 2017;151:268–81. https://doi.org/10.1016/j.compscitech.2017.08.031.

[30] Yang X, Du H, Li S, Wang Z, Shao L. Codepositing mussel-inspired nanohybrids onto one-dimensional fibers under "green" conditions for significantly enhanced surface/interfacial properties. ACS Sustain Chem Eng 2018;6:4412–20. https://doi.org/10.1021/acssuschemeng.8b00290.

[31] Wang X, Huang Z, Lai M, Jiang L, Zhang Y, Zhou H. Highly enhancing the interfacial strength of CF/PEEK composites by introducing PAIK onto diazonium functionalized carbon fibers. Appl Surf Sci 2020;510:145400. https://doi.org/10.1016/j.apsusc.2020.145400.

[32] Pearson A, Liao W, Kazemi Y, Duncan M, Slingerland E, Kakroodi A, et al. Fiber-matrix adhesion between high-density polyethylene and carbon fiber. Polym Test 2022;105:107423. https://doi.org/10.1016/j.polymertesting.2021.107423.

[33] Kaynak C, Orgun O, Tincer T. Matrix and interface modification of short carbon fiber-reinforced epoxy. Polym Test 2005;24:455–62. https://doi.org/10.1016/j.polymertesting.2005.01.004.

[34] Ghaffari S, Makeev A, Seon G, Cole DP, Magagnosc DJ, Bhowmick S. Understanding compressive strength improvement of high modulus carbon-fiber reinforced polymeric composites through fiber-matrix interface characterization. Mater Des 2020;193:108798. https://doi.org/10.1016/j.matdes.2020.108798.

[35] Piggott MR, Chua PS, Andison D. The interface between glass and carbon fibers and thermosetting polymers. Polym Compos 1985;6:242–8. https://doi.org/10.1002/pc.750060409.

[36] Favre JP, Perrin J. Carbon fibre adhesion to organic matrices. J Mater Sci 1972;7:1113–8. https://doi.org/10.1007/BF00550192.

[37] Yang L, Thomason JL, Zhu W. The influence of thermo-oxidative degradation on the measured interface strength of glass fibre-polypropylene. Compos Part A Appl Sci Manuf 2011;42:1293–300. https://doi.org/10.1016/j.compositesa.2011.05.011.

[38] Miller B, Muri P, Rebenfeld L. A microbond method for determination of the shear strength of a fiber/resin interface. Compos Sci Technol 1987;28:17–32. https://doi.org/10.1016/0266-3538(87)90059-5.

[39] Minty RF, Yang L, Thomason JL. The dependence of interfacial shear strength on temperature and matrix chemistry in glass fibre epoxy composites. Compos Part A Appl Sci Manuf 2023;164:107303. https://doi.org/10.1016/j.compositesa.2022.107303.
[40] Thomason J. An overview of some scaling issues in the sample preparation and data interpretation of the microbond test for fibre-matrix interface characterisation. Polym Test 2022;111:107591. https://doi.org/10.1016/j.polymertesting.2022.107591.
[41] Yang L, Thomason JL. Development and application of micromechanical techniques for characterising interfacial shear strength in fibre-thermoplastic composites. Polym Test 2012;31:895–903. https://doi.org/10.1016/j.polymertesting.2012.07.001.
[42] Minty RF, Thomason JL, Yang L, Stanley W, Roy A. Development and application of novel technique for characterising the cure shrinkage of epoxy resins. Polym Test 2019;73:316–26. https://doi.org/10.1016/j.polymertesting.2018.11.045.
[43] Tandon GP, Pagano NJ. Micromechanical analysis of the fiber push-out and re-push test. Compos Sci Technol 1998;58:1709–25. https://doi.org/10.1016/S0266-3538(98)00037-2.
[44] Kerans RJ, Parthasarathy TA. Theoretical analysis of the fiber pullout and pushout tests. J Am Ceram Soc 1991;74:1585–96. https://doi.org/10.1111/j.1151-2916.1991.tb07144.x.
[45] Ureña A, Rams J, Escalera MD, Sánchez M. Characterization of interfacial mechanical properties in carbon fiber/aluminium matrix composites by the nanoindentation technique. Compos Sci Technol 2005;65:2025–38. https://doi.org/10.1016/j.compscitech.2005.04.013.
[46] Rodríguez M, Molina-Aldareguía JM, González C, LLorca J. Determination of the mechanical properties of amorphous materials through instrumented nanoindentation. Acta Mater 2012;60:3953–64. https://doi.org/10.1016/j.actamat.2012.03.027.
[47] Broutman LJ. Measurement of the fiber-polymer matrix interfacial strength. Interfaces Compos 1969;452:27–41.
[48] Kelly A, Tyson WR. Tensile properties of fibre-reinforced metals–copper/tungsten and copper/molybdenum. J Mech Phys Solids n.d.;13.
[49] Stojcevski F, Hilditch TB, Gengenbach TR, Henderson LC. Effect of carbon fiber oxidization parameters and sizing deposition levels on the fiber-matrix interfacial shear strength. Compos Part A Appl Sci Manuf 2018;114:212–24. https://doi.org/10.1016/j.compositesa.2018.08.022.
[50] Piggott MR, Xiong Y. Direct observation of debonding in fiber pull-out specimens, fiber, matrix, and interface properties. Am Soc Test Mater Ed, ASTM STP 1996;1290:84–91.
[51] Kallas MN, Koss DA, Hahn HT, Hellmann JR. Interfacial stress state present in a "thin-slice" fibre push-out test. J Mater Sci 1992;27:3821–6. https://doi.org/10.1007/BF00545464.
[52] Minty RF, Yang L, Thomason JL. The influence of hardener-to-epoxy ratio on the interfacial strength in glass fibre reinforced epoxy composites. Compos Part A Appl Sci Manuf 2018;112:64–70. https://doi.org/10.1016/j.compositesa.2018.05.033.
[53] Ramaswamy K, Modi V, Rao PS, Martin PP, McCarthy CT, O'Higgins RM. An investigation of the influence of matrix properties and fibre–matrix interface behaviour on the mechanical performance of carbon fibre-reinforced PEKK and PEEK composites. Compos Part A Appl Sci Manuf 2023;165:107359. https://doi.org/10.1016/j.compositesa.2022.107359.
[54] Chawla V, Puplampu SB, Murray NJ, Penumadu D. Degradation in interfacial shear strength of carbon fiber/ vinyl ester composites due to long-term exposure to seawater using push-out tests. Compos Sci Technol 2023;241:110131. https://doi.org/10.1016/j.compscitech.2023.110131.
[55] Medinam C, Molina-Aldareguía JM, González C, Melendrez MF, Flores P, Llorca J. Comparison of push-in and push-out tests for measuring interfacial shear strength in nano-reinforced composite materials. J Compos Mater 2016;50:1651–9. https://doi.org/10.1177/0021998315595115.
[56] Zhandarov S, Mäder E. Characterization of fiber/matrix interface strength: applicability of different tests, approaches and parameters. Compos Sci Technol 2005;65:149–60. https://doi.org/10.1016/j.compscitech.2004.07.003.
[57] Zhang L, Ren C, Zhou C, Xu H, Jin X. Single fiber push-out characterization of interfacial mechanical properties in unidirectional CVI-C/SiC composites by the nano-indentation technique. Appl Surf Sci 2015;357:1427–33. https://doi.org/10.1016/j.apsusc.2015.10.018.
[58] Godara A, Gorbatikh L, Kalinka G, Warrier A, Rochez O, Mezzo L, et al. Interfacial shear strength of a glass fiber/epoxy bonding in composites modified with carbon nanotubes. Compos Sci Technol 2010;70:1346–52. https://doi.org/10.1016/j.compscitech.2010.04.010.
[59] Canal LP, González C, Segurado J, LLorca J. Intraply fracture of fiber-reinforced composites: microscopic mechanisms and modeling. Compos Sci Technol 2012;72:1223–32. https://doi.org/10.1016/j.compscitech.2012.04.008.
[60] Sha JJ, Dai JX, Li J, Wei ZQ, Hausherr J-M, Krenkel W. Measurement and analysis of fiber-matrix interface strength of carbon fiber-reinforced phenolic resin matrix composites. J Compos Mater 2014;48:1303–11. https://doi.org/10.1177/0021998313485264.
[61] Toray T700G Commercial Documentation n.d. https://toray-cfe.com/wp-content/uploads/2020/12/toray-torayca-t700g-haute-resistance.pdf (accessed April 5, 2024).
[62] Gholinia A, Donoghue J, Garner A, Curd M, Lawson MJ, Winiarski B, et al. Exploration of fs-laser ablation parameter space for 2D/3D imaging of soft and hard materials by tri-beam microscopy. Ultramicroscopy 2024;257:113903. https://doi.org/10.1016/j.ultramic.2023.113903.
[63] Gaitanelis D, Chanteli A, Worrall C, Weaver PM, Kazilas M. A multi-technique and multi-scale analysis of the thermal degradation of PEEK in laser heating. Polym Degrad Stab 2023;211:110282. https://doi.org/10.1016/j.polymdegradstab.2023.110282.
[64] Packham DE. Handbook of adhesion. Longman Scientific and Technical 1992.
[65] Brocks T, Cioffi MOH, Voorwald HJC. Effect of fiber surface on flexural strength in carbon fabric reinforced epoxy composites. Appl Surf Sci 2013;274:210–6. https://doi.org/10.1016/j.apsusc.2013.03.018.
[66] Dai Z, Shi F, Zhang B, Li M, Zhang Z. Effect of sizing on carbon fiber surface properties and fibers/epoxy interfacial adhesion. Appl Surf Sci 2011;257:6980–5. https://doi.org/10.1016/j.apsusc.2011.03.047.
[67] Wu Q, Li M, Gu Y, Wang S, Wang X, Zhang Z. Reaction of carbon fiber sizing and its influence on the interphase region of composites. J Appl Polym Sci 2015;132. https://doi.org/10.1002/app.41917.